RSC Advances

ROYAL SOCIETY OF CHEMISTRY

www.rsc.org/advances

RSC Advances

ARTICLE

Highly Selective and Efficient Adsorption Dyes Self-assembled by 3D Hierarchical Architecture of Molybdenum Oxide †

Received 00th January 20xx,
Accepted 00th January 20xx

DOI: 10.1039/x0xx00000x

www.rsc.org/

Min Wang,[a] Xiao-xiao Song,[a] Xiao-Li Cheng[a], Xin Zhou,[‡b] Xian-fa Zhang,[a] Zhuang Cai, Ying-Ming Xu,[*a] Shan Gao,[a] Hui Zhao,[a] Li-Hua Huo[*a]

A novel hierarchical architecture of molybdenum trioxide (α-MoO_3) was synthesized via a facile template-free hydrothermal route directly by using molybdenyl acetylacetonate and acetic acid as the starting materials. SEM and TEM observations indicate that this microstructure is a kind of flower-like microspheres with the diameter of 15 to 20 μm. It consists of numerous nanobelts with (001) preferential crystallographic plane which seemingly grow from the sphere-like core and the nanobelts were 100 nm in width, 4 μm in length and 15-20 nm in thickness. The molybdenum oxide-based hierarchical microstructure exhibits a fast and selective adsorption to the adsorbate organic pollutants with benzoic acidic group for the first time. The removal rate of α-MoO_3 to RhB reaches 97.9% in 10 min at a RhB concentration of 20 mg L^{-1} at room temperature, which is significantly fast as well as the commercial active carbon and the maximum adsorption capacity is 9 times that of the commercial activated carbon at a RhB concentration of 200 mg L^{-1}. The mechanism for selective adsorption was discussed according to the results of IR, XPS and theoretical calculation. XPS and IR spectra confirm the RhB molecules adsorbed on the surface of MoO_3 and interacted with Mo ions. DFT calculations indicate that the larger delocalization of the organic groups, the larger amount of charges transfer, the higher binding energy of organic molecules to the (001) lattice plane of α-MoO_3 surface.

Introduction

Synthetic dye is one of the representative organic pollutants originating from the chemical and textile industries. Water contaminated by synthetic dyes may induce mutagenic activity[1,2] and posed negative effects on aquatic life via obstructing light penetration and oxygen transfer into water bodies. It has been well-recognized that most synthetic dyes are highly recalcitrant to biodegradation because of their xenobiotic nature.[3] Therefore, removal of synthetic dyes from water prior to their discharge into the natural environment is very important to protect the environment. Among different methods available for the purification of dye polluted water, adsorption technique is a simple and widely used one,[4] in which activated carbons (AC) are most widely used as adsorbents for the treatment of polluted water.[5] However, some properties of AC, such as high regeneration temperature, nonselective and unsuitable hydrophilicity/hydrophobicity, limit the AC application in industrial field.[5,6] Recently, several groups reported that some transition metal oxide nanostructures with hierarchical microstructure, such as nickle oxide,[7] iron oxide,[8] tungsten oxide,[9] or with mesoporous structure, e.g. Cu_2O,[10] exhibited better removal ability for organic dyes in water by adsorption at room temperature. The tungsten oxide could be regenerated and the regenerated oxides kept almost the same adsorption performance to methylene blue.[9] However, the adsorption capacities of most of the transition metal oxide nanostructures are lower than those of the activated carbons, except the urchin-architectured Cu_2O to methyl orange.[10]

Recently, selective adsorption is being a new attractive field applied for separation of mixed gases[11] and bioactive materials.[12] Little attention has been concentrated on selective adsorption for dyes. Activated carbon has good adsorption effect on most dyes, but it can not effectively separate the target pollutions. Therefore, it is of great importance to find and prepare selective adsorbents for removing certain pollutants in water. The pollutants can be easily desorbed from the adsorbents by simple method for recycling usage. Only Peng et al. reported that the transition metal oxide, ZnO nanoporous pyramid[13] showed better adsorption capacity than AC and good selectivity to acid dyes due to its more basic sites on its surfaces. Therefore, exploring selective adsorbents with high adsorption capacity to different dyes remains a major challenge.

Molybdenum trioxide (α-MoO_3), as a wide band gap n-type semiconductor with layered crystal structure, is one of the most intriguing transition metal oxides with distinctive functional properties over the past decades because of its non-toxic nature and low-cost. Especially nanostructured MoO_3 has been widely

[a] *Key Laboratory of Functional Inorganic Material Chemistry, Ministry of Education, School of Chemistry and Materials Science, Heilongjiang University, Harbin 150080, People's Republic of China. E-mail address: xuyingming@hlju.edu.cn; lhhuo68@yahoo.com;Tel.: (+86) 0451-86608426; Fax: (+86) 0451-86608040.*
[b] *Laboratory Centre of Pharmacy, College of Pharmacy Harbin Medical University, Harbin 150081, People's Republic of China*
[‡] *The first author of theoretical calculation*
† Electronic Supplementary Information (ESI) available: Additional Figures and PXRD patterns for all co-crystals. Crystallographic files for **1-4** in cif format. See DOI: 10.1039/x0xx00000x

investigated and applied in the fields of electrochromism/photochromism devices,[14] smart windows,[15] gas sensors,[16] field emission devices,[17] capacitors,[18] catalysts[19] and lithium-ion battery.[20] However, there is few report about the separation properties of α-MoO_3 to dyes. Normally, the performances of nanomaterials strongly depend on the special microstructure and morphologies.[21-27] The above researches on the adsorption performance of nanostructured transition metal oxides suggest that the hierarchical structures with nanometer-sized building blocks (especially 1D construction unit) could provide a high surface-to-bulk ratio, or with suitable surface functional groups or preferential crystallographic planes could easily interact with pollutants in favor of dye adsorption. Furthermore, the overall micrometer-sized structure could also offer desirable mechanical strength, easy separation and recovery. It is possible to design and explore a new adsorbent of MoO_3 with good adsorption capacity and selectivity to certain dye via constructing a novel hierarchical microstructure based on 1D building block with certain preferential crystallographic plane.

Substantial efforts have been focused on the controllable synthesis of molybdenum oxide-based hierarchical microstructures recently. Till now, hierarchical MoO_3 with 1D building blocks has been synthesized by flame,[28] vapor transport,[29] electrodeposition[30] and hydrothermal methods,[31] among which hydrothermal technique was mainly used for synthesis of hierarchical MoO_3 with different morphology. MoO_3 multilamellar fibers based on nanofibers were obtained by a surfactant-templated hydrothermal process at 180°C for 4 d.[31a] In the presence of cetyltrimethyl ammonium bromide, Zhang et al. also prepared the hierarchical MoO_3 flowers assembled by nanobelts at 180°C.[31b] Without any template addition, cross-like nanoflower MoO_3 architecture based on nanoplates could be synthesized via a simple solution-based route at 180°C,[31c] and MoO_3 nanoflowers could be assembled by nanobelts via microwave hydrothermal procedure.[31d] Recently, Zhang et al. reported that different hierarchical morphology with different building blocks, including urchin-shape MoO_3, could be obtained by controlling the hydrothermal synthesis conditions and additives in the temperature range of 65-75°C.[31e] Mesoporous spheres based on nanorod construction unit could be obtained using formaldehyde as the capping agent at 120°C.[31f] Therefore, develop a facile template-free low temperature route to synthesize novel hierarchical MoO_3 with 1D building blocks, especially with preferential crystallographic planes at the same time, is highly desirable.

In this paper, novel α-MoO_3 hierarchical microstructures, based on nanobelts with (001) preferential crystallographic plane, were synthesized by a facile hydrothermal method at low temperature without any template addition. The excellent ability of α-MoO_3 to selectively remove organic dyes with benzoic acidic group for water treatment was reported for the first time. It could be a promising separation material applied for rapid removal of organic pollutants in water. The selective adsorption mechanism of such hierarchical structure α-MoO_3 to Rhodamine B was discussed by IR, XPS and theoretical calculation in detail.

Experimental

Preparation of α-MoO_3 hierarchical architecture

All reagents were of analytical grade and used as received without further purification. The detailed synthesis process is as follows: 0.114 g molybdenyl acetylacetonate ($C_{10}H_{14}MoO_6$) was dissolved in 35 mL of acetic acid under magnetic stirring. After stirring for 30 min, the obtained transparent solution was transferred and sealed in a Teflon-lined stainless autoclave with a capacity of 50 mL. The autoclave was heated to 150°C and held for 8 h, then allowed to cool to room temperature. The precipitate was washed several times with distilled water and absolute ethanol, respectively, and then dried at 60°C for several hours and kept in dessicator for further characterization.

Characterization

Phase and crystalline of the as-synthesized product and the corresponding powders annealed at 250°C for 1 h in air were determined by X-ray powder diffractometer (XRD) (Rigaku, D/MAX-3B) with Cu Kα radiation (λ=0.15405 nm). Morphology and microstructure of the samples were observed by scanning electron microscope (SEM) (FEI/Philips, XL-30). TEM, HRTEM and SAED images were obtained on transmission electron microscope (JEOL, JEM-2100, Japan). Fourier transform infrared spectra (FT-IR) of the samples were recorded with KBr pellets using a FT-IR spectrometer (Bruker Equinox, 55) with a mercury-cadmium-telluride (MCT) detector. TUV-Vis spectra of the samples were recorded on a UV-Vis spectrophotometer (Perkin Instrument, Lambda 900) at room temperature. The X-ray photoelectron spectroscopy (XPS) spectra of the samples were recorded on a Kratos Axis Ultra Dld photoelectron spectrometer equipped with monochromatic Al-Kα radiation. In order to calculate the binding energies, the C 1s peak of the C-(C, H) component at 284.6 eV was used as an internal standard. The XPS peaks were fitted by a Gaussian and Lorentzian sum function using XPS Peak 4.1 Freeware.[32] The specfic surface was calculated from a nitrogen adsorption-desorption analysis conducted at 77K using Brunauer-Emmett-Teller (BET, Tristar 3020, Micrometrics, USA).

Water treatment experiments

In the water-treatment experiments, Rhodamine B (RhB) was employed as the probe of organic pollutants in aqueous solution. In a typical experiment, 20 mg α-MoO_3 nanoflowers heat-treated at 250°C was dispersed into 20 mL RhB aqueous solution with different concentrations (20-200 mg L^{-1}) , which was then kept stirring at room temperature. At a preset time interval, 2 mL aliquots were sampled and centrifuged at 10000 rpm for 3 min to remove the adsorbent. At last, the supernatant liquid was drawn off and analyzed using a UV-Vis spectrophotometer to determine the remaining concentration of RhB solution at λ=554 nm by standard spectrophotometric method. The adsorption isotherms of RhB were obtained by varying the initial concentration of RhB solutions at room temperature. Activated carbon was served as the reference to compare the adsorption ability under the same experimental conditions. Furthermore, we also studied the adsorption

performances of the above sample to other eight organic dyes at a dye concentration of 20 mg L^{-1}, the adsorption processes were carried out in the same experimental conditions with those of RhB solution.

Computational details

The calculations were performed with VASP package[33-35] with projector augmented wave (PAW) pesudopotentials. The exchange-correlation functional utilized was at the generalized gradient approximation level, known as GGA-PBE.[36] A plane-wave basis set with a cutoff energy of 400 eV was used for electron wave function. A Monkhost_Pack mesh of 3×3×1 k-points was used for sampling the Brillouin zone during ionic relaxation, which is large enough for the current simulation. Optimization of structures was converged until the force on each atom is less than 1×10^{-3} eV nm^{-1}, and energies were converged to 1×10^{-5} eV. In this work, 15.85 Å × 13.86 Å × 20.00 Å is chosen for the supercell of MoO_3 cell, the large vacuum space used in the supercells can avoid the interaction between the surface cells and their images along the z-axes.

The binding energy (Ebinding) between organic molecules and the surface of MoO_3 was defined as:

$E_{binding} = E(Org + MoO_3) - E(MoO_3) - E(Org)$

Where $E(Org + MoO_3)$ is the total energy of the MoO_3 with an organic molecule adsorbed, and $E(MoO_3)$ and E(Org) are the total energy of the MoO_3 and organic molecule, respectively.

Results and discussion

Morphology and structural properties

Fig. 1 presents typical SEM images of the as-synthesized product. From the low-magnification SEM image (Fig. 1a), it can be seen that the sample is a hierarchical architecture of flower-like microspheres, with the diameters of 15 to 20 μm. Such large size of the microspheres would be fairly easy for the adsorbent/liquid separation after dyes adsorption. The high-magnification SEM image of a typical microsphere (Fig. 1b and c) illustrates that the assembly of flower-like nanostructures consists of numerous nanobelts which are 100 nm in width, 4 μm in length and 15-20 nm in thickness. These high-density nanobelts seemingly grow from the sphere-like core, with the diameters of 15 to 20 μm and present sharp tips and rough edges. The product calcined at 250°C also shows the same morphology (Fig. S1).

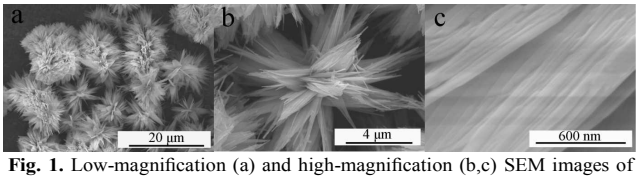

Fig. 1. Low-magnification (a) and high-magnification (b,c) SEM images of the as-synthesized MoO_3 flower-like microspheres.

Further characterization of the flower-like microspheres was performed by means of TEM. The typical TEM images of the as-synthesized product are depicted in Fig. 2. It also clearly reveals that the hierarchical architecture is constructed by numerous nanobelts in nature (Fig. 2a) which presents the same information with those observed from SEM images. From Fig. 2b, it can be seen that the branches of the flower-like microspheres are constructed from nanobelts. Fig. 2c shows the HRTEM image of the edge of a single nanobelt. The clear lattice fringes with interplanar spacing of about 0.36 nm can be observed, which corresponds well to the (001) lattice plane of α-MoO_3.[37] The selected area electron diffraction (SAED) pattern of individual α-MoO_3 nanobelt is given in the inset of Fig. 2c. It is composed of a highly-ordered diffractional lattice with a large and homogeneous diffraction dot array, suggesting the single-crystalline nature of α-MoO_3 nanobelt with high crystallinity. The SAED pattern also recorded perpendicular to the growth axis of a single nanobelt which can be indexed to the (010) zone axis of α-MoO_3, implying preferential growth along the c-axis or (001) direction, which is consistent with HRTEM result.[38] The specific surface area is thus evaluated to be 17.7 m^2 g^{-1} from data points in the pressure range by the Brunauer-Emmett-Teller (BET) equation, which is higher than that of the reported nanomaterials of MoO_3.[38] The nitrogen adsorption-desorption isotherms of nanoflower-like α-MoO_3 is shown in Fig. S2.

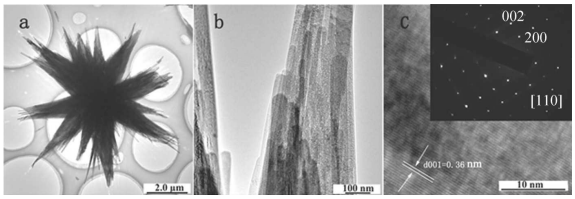

Fig. 2. TEM (a, b), HRTEM (c) images and SAED pattern (inset of c) of the as-synthesized MoO_3 flower-like microspheres.

The XRD patterns of the as-synthesized α-MoO_3 and product after calcined at 250°C are shown in Fig. 3. For the as-synthesized sample (Fig. 3a), several characteristic diffraction peaks are seen, the calculated d-values are in agreement with those given in the standard data of α-MoO_3 (JCPDS 05-0508).[37] No characteristic peaks are observed for other impurities, indicating that pure α-MoO_3 has been obtained before calcination. After the sample calcined at 250°C for 1 h in air (Fig. 3b), a few new diffraction peaks appear, still corresponding to the orthorhombic MoO_3, and the intensity of

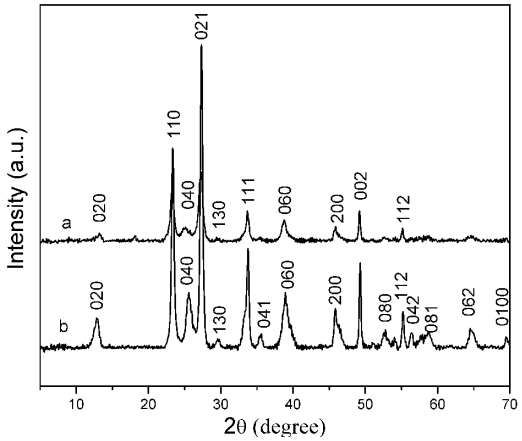

Fig. 3. XRD patterns of the as-synthesized product (a) and the sample after calcined at 250 °C for 1 h in air (b).

other diffraction peaks of α-MoO_3 increases. It shows that the flower-like microspheres crystallize better after calcination.

IR spectra analysis also confirms the formation of layered α-MoO_3 phase in the hierarchical architecture. Fig. 4 shows the FT-IR spectra of the as-synthesized sample (Fig. 4a) and the product after calcined at 250°C for 1 h in air (Fig. 4b). It can be seen that there are four absorption bands at 552, 836, 995 and 1603 cm^{-1}, respectively in the IR spectrum of the as-synthesized sample. The band located at 552 cm^{-1} is due to the bending vibration of the Mo-O-Mo entity where each O^{2-} ion is shared by three Mo^{6+} ions.[39] The absorption band at 836 cm^{-1} is attributed to the Mo-O-Mo vibration of Mo^{6+}.[40] The band at 995 cm^{-1} is assigned to the terminal Mo=O stretching vibration mode, which is an indicator of the layered orthorhombic MoO_3.[41] The small band at 1603 cm^{-1} is assigned to the bending vibration of water, indicating small quantity of water existence in the interlayers of MoO_3. After calcination, only the bands related to the molybdenum oxide exist, indicating the interlayered water removal.

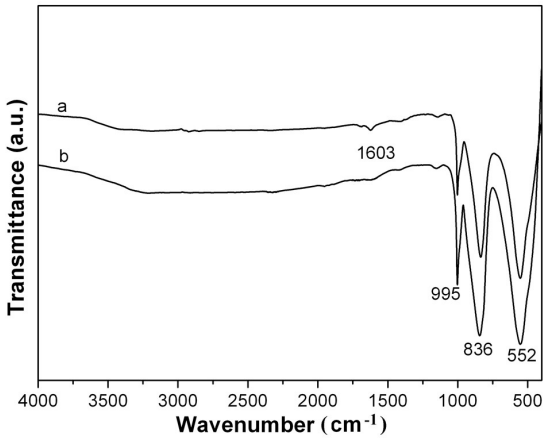

Fig. 4. IR spectra of the as-synthesized product (a) and the sample after calcined at 250 °C for 1 h in air (b).

Adsorption properties in water treatment

The heat-treated α-MoO_3 flower-like microspheres were tested as adsorbent for waste water treatment. Fig. 5 shows the adsorption curves measured with different RhB concentrations of 20-200 mg L^{-1} at room temperature. It can be seen that the adsorption rate of commercial AC is faster than that of α-MoO_3 flower-like microspheres at low RhB concentrations (20 and 60 mg L^{-1}), and the removal rate of AC is slightly higher than that of α-MoO_3 (Fig. 5a and b). For example, at an RhB concentration of 20 mg L^{-1} (shown in Fig. 5a), it takes 5 min for AC to reach the adsorption/desorption equilibrium but α-MoO_3 needs 10 min. At a higher concentration of 100 mg L^{-1}, the adsorption rate of AC is still faster than that of α-MoO_3 at first, but the adsorption rate of α-MoO_3 is faster than that of AC after 1400 min, while the removal rate of α-MoO_3 was slightly higher than that of AC (Fig. 5c). However, when the RhB concentration increases to 200 mg L^{-1}, the α-MoO_3 exhibits both higher adsorption rate and larger removal capacity than those of AC (Fig. 5d). For example, at a RhB concentration of 200 mg L^{-1} (Fig. 5 d), the adsorption rate of AC is faster than that of α-MoO_3 within first 290 min, but the adsorption rate of α-MoO_3 is faster than that of AC after 1010 min. After adsorption for 290 min, the removal rate of AC remains almost the same and the maximum removal rate is only 10%, while that of the α-MoO_3 microspheres still increases with the adsorption times increasing and reaches to maximum 90.5% till 3800 min adsorption at the adsorption/desorption equilibrium. It means that the remaining concentration of RhB lowers to 9.5%, and the adsorption capacities of α-MoO_3 microspheres is about 9 times that of commercial activated carbon. It shows that such α-MoO_3 microspheres are suitable to remove RhB in the polluted water with high concentrations.

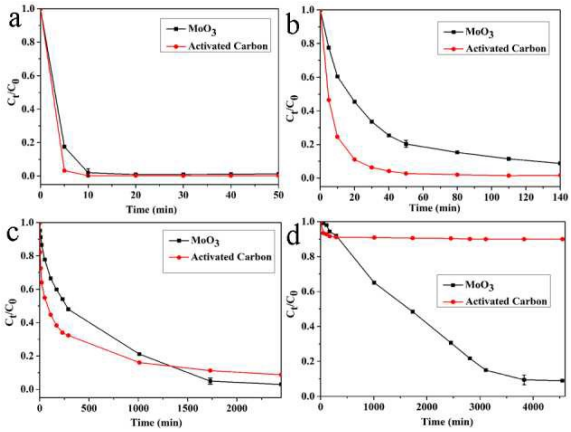

Fig. 5. Adsorption curves of the aqueous RhB with different concentrations in the presence of α-MoO_3 and activated carbon at different intervals (a: 20, b: 60, c: 100, d: 200 mg L^{-1}).

The relationship between the removal ability of the material and the concentration of the contaminant solution is illustrated by the adsorption isotherm. Fig. 6 shows the adsorption isotherm of RhB for the tested molybdenum oxide microspheres. A Langmuir adsorption model is used to represent the relationship between the amount of RhB adsorbed at equilibrium (q_e, mg g^{-1}) and the equilibrium solution concentration (C_e, mg L^{-1}),

$$1/q_e=(1 + bC_e) / q_m\, b\, C_e$$

where q_m (mg g^{-1}) is the maximum adsorption capacity corresponding to complete monolayer coverage and b is the

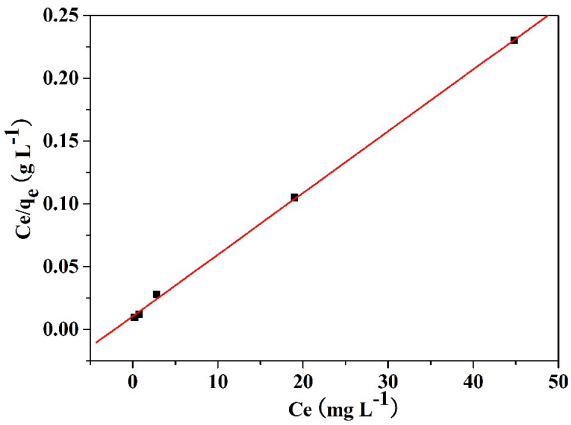

Fig. 6. The adsorption capacities of α-MoO_3 with RhB as pollutant using the Langmuir adsorption model.

equilibrium constant (L mg^{-1}). The $1/q_e$ and $1/C_e$ are obtained after the adsorption process reaches the equilibrium state. As shown in Fig. 6, it is clearly found that the experimental data fit well with the Langmuir adsorption model. The maximum adsorption capacity of MoO_3 microspheres can be calculated as about 204.08 mg g^{-1}, which is 9 times of the AC (20 mg g^{-1}).

For comparison, we also studied the adsorption performance of commercial α-MoO_3 (SEM image shown in Fig. S3) at a RhB concentration of 100 mg L^{-1} (shown in Fig. 7). Under the same experimental conditions, the remaining concentration of RhB of commercial α-MoO_3 is higher than that of hierarchical architecture after 290 min. It suggests that the removal rate of the flower-like microspheres is higher than that of commercial α-MoO_3 aggregates. In other words, the corresponding removal rate of commercial α-MoO_3 and microspherical α-MoO_3 are about 14.7% and 52.0%, respectively. Such a performance can also be confirmed when the adsorption time is prolonged to 1730 min. This difference is possible because that this hierarchical micro/nanostructures assembled by nanobelts building blocks can provide large surface areas and numerous activated sites for the adsorption of organic pollutants. This suggests that the as-prepared α-MoO_3 flower-like microspheres are a new and efficient adsorbent material for organic wastewater treatment application.

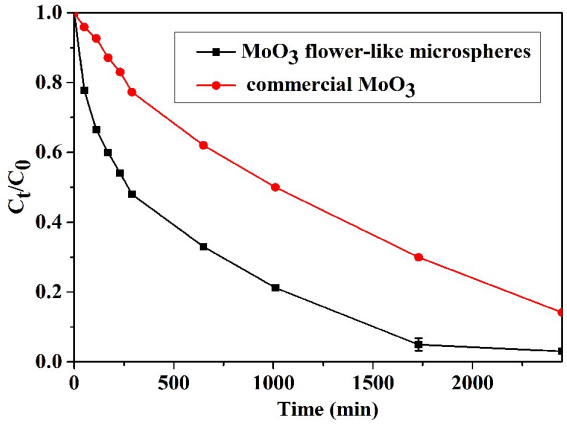

Fig. 7. Adsorption curves of the aqueous RhB with the same concentration (100 mg L^{-1}) in the presence of commercial α-MoO_3 (a) and α-MoO_3 microspheres (b) at different intervals.

In order to study the recycle performances of the samples, the flower-like MoO_3 microspheres were circularly used 5 times. After one cycle of adsorption measurement, the adsorbents were collected, dried and annealed at 250°C for 30 min and the as-obtained samples were further used in a new cycle of adsorption (the recyclable performance shown in Fig. S4). After regenerating five times, the removal percentage of RhB is still over 98%. Hardly any decay of the removal efficiency can be observed, indicating a good adsorption recyclability of such 3D MoO_3 microspheres. Furthermore, the dyes can be easily desorbed from the surface of MoO_3 even by ethanol washing at room temperature. The desorption efficiency of RhB after adsorption with the ethanol washed 3D MoO_3 nanostructured sample is still 70%. The color of the MoO_3 powder before and after adsorption of RhB changes from hoary to purple. After ethanol washing, the surface of MoO_3 becomes lilac color (Fig. S5).

The selective adsorption capability of 3D α-MoO_3 microspheres were further studied by comparing the adsorption performance of these microspheres to other eight dyes (including methyl blue, fuchsine, cresol red, methyl orange, xylenol orange, alizarin red, alizarin yellow R, and methyl red) at a dye concentration of 20 mg L^{-1}, which carried out in the same experimental conditions. Fig. 8 shows the selective adsorption results of α-MoO_3 nanostructures to nine dyes. It is quite clear that α-MoO_3 microspheres can adsorb more than 99% of RhB, alizarin yellow R and MR in 30 minutes, but shows almost no adsorption to methyl blue, fuchsin, cresol red, methyl orange, xylenol orange and alizarin red. According to the molecular structure analysis, it is found that the benzoic acidic group exists in the adsorbed RhB, alizarin yellow R and methyl red (see Fig. S6). The effect of solution pH on adsorption is presented in Fig. S7. It is shown that solution pH (3-10) exerts a little effect on RhB adsorption.

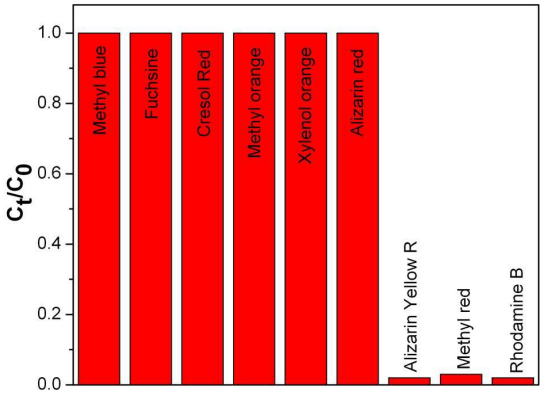

Fig. 8. Selective adsorption of α-MoO_3 to nine dyes.

Adsorption mechanism discussion

Compared to the (010) and (100) surface of MoO_3, the (001) surface of MoO_3 has the strongest interaction with carboxylic acid (Fig. S8 and S9). Therefore, we only discuss the selective adsorption case of the (001) surface. To prove the selective adsorption of benzoic acid to the surface of MoO_3 (001), C_6H_5COOH, $C_6H_5SO_3H$ and $C_6H_5CH_2NHCOOH$ were selected as the dye models to simulate the adsorption of RhB, alizarin red and xylenol orange onto the surface of MoO_3 (001). For bare MoO_3 (001), there are three types of coordination unsaturated sites, namely the bridging O (O_{br}), terminal O (O_{ter}) and five-coordinated Mo (Mo_{5c}), therefore, three adsorption-types of the organic molecules were taken into account in this simulation, the optimized structures of which are shown in Fig. 9. With respect to all of the three organic molecules, the binding energies of which adsorbed onto Mo5c are larger than those adsorbed onto O_{br}, this is due to the formation of the coordination bond between the oxygen atom (org) and Mo_{5c}, while the character of bonding between O_{br} and H (org) is hydrogen bond. The case of $C_6H_5SO_3H$-MoO_3 (001) is different from the others, where the hydrogen atom of SO_3H group is away from the surface of MoO_3, this is because the real dye

investigated in experiments is R-$C_6H_5SO_3Na$ and Na ion will never be adsorbed onto the surface of MoO_3 (001). The binding energies of the three most stable structures are −1.62 eV (C_6H_5COOH), −1.33 eV ($C_6H_5SO_3H$) and −1.07 eV ($C_6H_5CH_2NHCOOH$), respectively, the largest binding energy of −1.62 eV indicates the stronger adsorption ability of C_6H_5COOH to MoO_3 (001) compared with the other two molecules. This corresponds to the observed selective adsorption of R-C_6H_5COOH molecules, the unique selectivity of which is resulted from the delocalized π bonding in C_6H_5COOH and the charge transfer from organic molecules to MoO_3 (001). To evaluate the effect of charge transfer, the charge on the investigated system was analyzed by the Bader scheme.[42,43] The Bader results indicate that the charge transfer from the organic molecules to MoO_3 is 0.20e (C_6H_5COOH), 0.16e ($C_6H_5SO_3H$) and 0.14e ($C_6H_5CH_2NHCOOH$), respectively. The large value implies the adsorption of the organic molecules is the nature of charge transfer and it can be concluded that the larger delocalization of the organic groups, the larger amount of charges transfer, the higher binding energy of organic molecules to the surface of MoO_3 (001). Therefore, this molybdenum oxide-based hierarchical microstructure exhibits selective adsorption to the organic pollutants with benzoic acidic group.

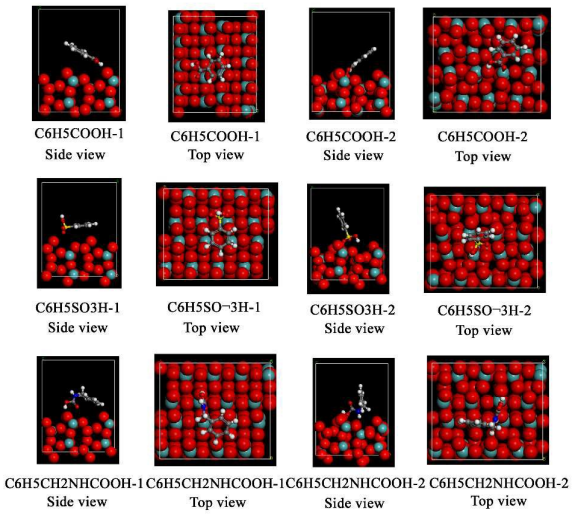

Fig. 9. Two kinds of adsorption structures of C_6H_5COOH, $C_6H_5SO_3H$ and $C_6H_5CH_2NHCOOH$ onto the MoO_3 (001) surface from the side and top view, respectively.

XPS and FT-IR analyses were also used to investigate the adsorption mechanism of MoO_3 to RhB. The Mo 3d and C 1s XPS spectra of MoO_3 microspheres before and after adsorption of RhB are given in Fig. 10. Comparing with the C 1s spectrum of the MoO_3 microspheres (Fig. 10a), the C 1s core-level spectrum of MoO_3 after RhB adsorption (Fig. 10b) is asymmetric and can be curve-fitted into five peak components at about 284.6, 285.7, 286.6, 287.8 and 289.8 eV, which can be attributed to the C-H/C-C, C-N, C-O, C=N[44] and O=C-O species, respectively.[45] This result indicates that the RhB has been adsorbed on the surface of the MoO_3. From Fig. 10c, it can be seen that there are two symmetric peaks at 232.2 and 235.3 eV, corresponding to Mo3d5/2 and Mo3d3/2 of Mo^{6+} of MoO_3. After adsorption of RhB (Fig. 10d), the peaks of Mo3d shift to lower binding energy obviously and a shoulder peak can be observed as shown in Fig. 10d, which suggests that there are two kinds of molybdenum species in the adsorbed sample. Through deconvolution of the XPS spectrum, four peaks can be obtained in which the peaks at 232.2 and 235.3 eV are associated with the characteristic peaks of Mo6+ of MoO_3, while the peaks at 230.3 and 233.4 eV can be attributed to the +4 valence state of Mo. It indicates the coordination of some molybdenum ions with the adsorbed RhB molecules on the surface of flower-like MoO_3 microspheres. This is in good accordance to the analysis of theoretical calculation.

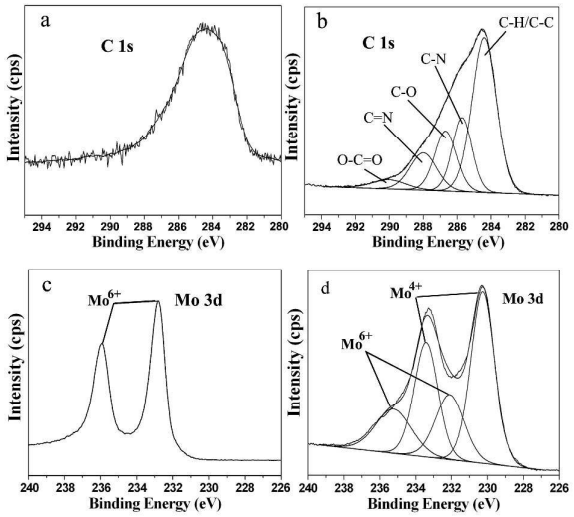

Fig. 10. The C 1s (a, b) and Mo 3d (c, d) XPS spectra of α-MoO_3 microspheres before (a, c) and after (b, d) RhB adsorption.

FT-IR spectra of RhB and α-MoO_3 microspheres before and after adsorption of RhB are shown in Fig. 11. It can be seen that new peaks appeared at 1100–1750 cm^{-1} corresponding to the vibrations of RhB molecules after α-MoO_3 microspheres adsorption of RhB, indicating the RhB molecules adsorbed on

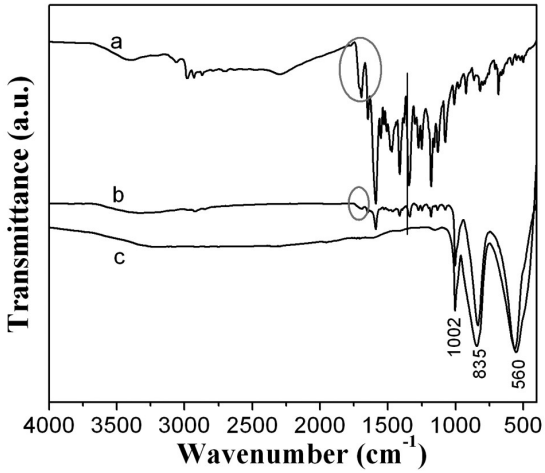

Fig. 11. IR spectra of the RhB (a), α-MoO_3 microspheres adsorbed RhB (b) and α-MoO_3 microspheres (c).

α-MoO_3 surface. The peak intensities of the adsorbed RhB molecules are decreased with different proportion. Especially, the peak of the -C=O vibration in the carboxyl group at 1710 cm^{-1} [46] becomes widen and weakened obviously compared with that of the benzene at 1589 cm^{-1} [47] after RhB adsorption (see the circle part in Fig. 11), indicating that the carboxyl group interacted with α-MoO_3. It further proves the above analysis results. All the above analysis results suggest that the selective adsorption of α-MoO_3 microspheres to RhB is attributed to the Mo ions coordination with the benzoic acidic group of organic molecules on (001) lattice plane of α-MoO_3 surface.

Conclusions

A unique α-MoO_3 hierarchical microspherical structure, about 10-15 μm size, with 1D nanobelts as building blocks and (001) preferential crystallographic plane, was directly synthesized by a facile solvothermal route without adding any surfactants or templates. Such large size of microspheres were employed to selective adsorb dyes with benzoic acidic group for the first time. It is found that the special MoO_3 microstructure exhibits a fast, selective and high adsorption capacity to the adsorbates compared with commercial active carbon and some other nanostructures of metal oxides. DFT calculations, XPS and IR analyses suggest that the selective adsorption is attributed to the Mo coordination with the benzoic acidic group of organic molecules on (001) lattice plane of α-MoO_3 surface. In a word, such flower-like microspheres are a new promising material for environmental remediation. It is also expected to be applied as special catalysts and gas sensing material.

Acknowledgements

This work was financial supported by the National Natural Science Foundation of China (21547012, 61271126, 21201060 and 21305033), Program for Innovative Research Team in University (IRT-1237), Program for Science and Technology Project of Heilongjiang province (B201414), Heilongjiang Educational Department (2013TD002, 12531506, 12541613), Youth Foundation of Harbin (2015RQQXJ047).

Notes and references

1 G. Lian, X. Zahng, S. J. Zhang, D. Liu, D. L. Cui and Q. L. Wang, *Energy Environ. Sci.,* 2012, **5**, 7072
2 C. S. Shen, Y. Shen, Y. Z. Wen, H. Y. Wang and W. P. Liu, *Water Res.*, 2011, **45**,5200
3 A. Pandey, P. Singh and L. Iyengar, *Int. Biodeterior. Biodegrad.*, 2007, **59**, 73
4 A. T. Nikolina, Z. K. George, K. L. Nikolaos and A. D. Eleni, *Langmuir.,* 2013, **29**, 1657; W. Cai, J. Yu and M. Jaroniec, *J. Mater. Chem*., 2010, **20**, 4587; J. Liu, S. B. Hartono, Y. G. Jin, Z. Li, G. Q. Lu and S. Z. Qiao, *J. Mater. Chem.*, 2010, **20**, 4595
5 O. Hernandez-Ramirez and S. M. Holmes, *J. Mater. Chem.*, 2008, **18**, 2751
6 E. Sabio, E. González, J. F. González, C. M. González-García, A. Ramiro and J. Ganan, *Carbon*, 2004, **42**, 2285
7 L. X. Song, Z. K. Yang, Y. Teng, J. Xia and P. Du, *J. Mater. Chem. A.,* 2013, **1**, 8731; T. Zhu, J. S. Chen and X. W. Lou, *J. Phys. Chem. C*., 2012, **116**, 6873
8 D. Z. Zhu, J. Zhang, J. M. Song, H. S. Wang, Z. Yu, Y. H. Shen and A. J. Xie, *Appl. Surf. Sci.,* 2013, **284**, 855
9 B. X. Liu, J. S. Wang, J. S. Wu, H. Y. Li, Z. F. Li, M. L. Zhou and T. Y. Zuo, *J. Mater. Chem. A.,* 2014, **2**, 1947
10 Y. Shang, D. F. Zhang and L. Guo, *J. Mater. Chem.*, 2012, **22**, 856
11 S. M. Kuznicki, V. A. Bell, S. Nair, H. W. Hillhouse, R. M. Jacubinas, C. M. Braunbarth, B. H. Toby and M. Tsapatsis, *Nature*, 2001, **412**, 720
12 K. Ariga, A. Vinu, M. Miyahara, J. P. Hill and T. Mori, *J. Am. Chem. Soc.*, 2007, **129**, 11022
13 Y. X. Liu, J. X. Shi, Q. Peng and Y. D. Li, *J. Mater. Chem.*, 2012, **22**, 6539
14 N. A. Chernova, M. Roppolo, A. C. Dillon and M. S. Whittingham, *J. Mater. Chem.*, 2009, **19**, 2526; A. Gavrilyuk, U. Tritthart and W. Gey, *Sol. Energy Mater. Sol. Cells.,* 2011, **95**, 1846
15 L. Zheng, Y. Xu, D. Jin and Y. Xie, *Chem. Mater.*, 2009, **21**, 5681
16 L. L. Sui, Y. M. Xu, X. F. Zhang, X. L. Cheng, S. Gao, H. Zhao, Z. Cai and L. H. Huo, *Sens. Actuators. B.,* 2015, **208**, 406; M. B. Rahmani, S. H. Keshmiri, J. Yu, A. Z. Sadek, L. Al-Mashat, A. Moafi, K. Latham, Y. X. Li, W. Wlodarski and K. Kalantarzadeh, *Sens. Actuators. B*., 2010, **145**, 13
17 A. Khademi, R. Azimirad, A. A. Zavarian and A. Z. Moshfegh, *J. Phys. Chem. C.*, 2009, **113**, 19298
18 T. Brezesinski, J. Wang, S. H. Tolbert and B. Dunn, *Nat. Mater.*, 2010, **9**, 146
19 L. X. Song, M. Wang, S. Z. Pan, J. Yang, J. Chen and J. Yang, *J. Mater. Chem.,* 2011, 21, 7982; S. M. Kemdeo, V. S. Sapkal and G. N. Chaudhari, *J. Mol. Catal. A: Chem.,* 2010, **323**, 70
20 S. M. Paek, J. H. Kang, H. Jung, S. J. Hwang and J. H. Choy, *Chem. Commun.*, 2009, 7536; Z. Y. Wang, S. Madhavi and X. W. Lou, *J. Phys. Chem. C.,* 2012, **116**, 12508;M. F. Hassan, Z. P. Guo, Z. Chen and H. K. Liu, *J. Power Sources*, 2010, **195**, 2372
21 H. H. Zhang, F. Zhou, M. Liu, D. L. Liu, D. D. Men, W. P. Cai ,G. T. Duan and Y. Li, *Adv. Mater. Interfaces*, 2015, **2**, 1500031
22 Y. Li, G. T. Duan, G. Q. Liu and W. P. Cai, *Chem. Soc. Rev.*, 2013, **42**, 3614
23 D. F. Zhang, H. Zhang, L. Guo, K. Zheng, X. D. Han and Z. Zhang, *J. Mater. Chem*., 2009, **19**, 5220
24 A. Baiker, P. Dollenmeier and A. Reller, *J. Catal.*, 1987, **103**, 394
25 A. M. Taurino, A. Forleo, L. Francioso, P. Siciliano, M. Stalder and R. Nesper, *Appl. Phys. Lett*., 2006, **88**, 152111.
26 W. Y. Li, F. Y. Cheng, Z. L. Tao and J. Chen, *J. Phys. Chem. B*., 2006, **110**, 119
27 J. G. Liu, Z. J. Zhang, C. Y. Pan, Y. Zhao, X. Su, Y. Zhou and D. P. Yu, *Mater. Lett.*, 2004, **58**, 3812
28 L. L. Cai, P. M. Rao and X. L. Zheng, *Nano Lett.*, 2011, **11**, 872
29 P. Badica, *Crystal Growth Design*, 2007, **7(4)**, 794
30 Y. C. Mao, W. Li, X. F. Sun, Y. J. Ma, J. Xia, Y. F. Zhao, X. H. Lu, J. Y. Gan, Z. Q. Liu, J. Chen, P. Liu and Y. X. Tong, *CrystEngComm*, 2012, **14**, 141
31 (a) R. Q. Song, A. W. Xu, B. Deng and Y. P. Fang, *J. Phys. Chem. B.*, 2005, **109**, 22758; (b) S. T. Wang, Y. G. Zhang, X. C. Ma, W. Z. Wang, X. B. Li, Z. D. Zhang and Y. T. Qian, *Solid State Commun.*, 2005, **136**, 283; (c) G. C. Li, L. Jiang, S. P. Pang, H. R. Peng and Z. K. Zhang, *J. Phys. Chem. B.*, 2006, **110**, 24472; (d) G. D Wei, W. Q. Qin, D. S. Zhang, G. F. Wang, R. Kim, K. Z. Zheng and L. L. Wang, *J. Alloys Comp.*, 2009, **481**, 417; (e) L. Fang , Y. Y. Shu, A. Q. Wang

and T. Zhang, *J. Cryst. Growth*, 2008, **310**, 4593; (f) Y. Shen, R. Huang, Y. Y. Cao and P. P. Wang, *Mater. Sci. Eng. B*, 2010, **172**, 237
32 R. W. M. Kwok, XPS peak freeware.
33 G. Kresse and J. Hafner, *Phys. Rev. B*, 1993, **47**, 558
34 G. Kresse and J. Hafner, *Phys. Rev. B*, 1994, **49**, 14251
35 G. Kresse and J. Furthmuller, *Phys. Rev. B*, 1996, **54**, 11169
36 J. P. Perdew, A. Ruzsinszky, G. I. Csonka, O. A. Vydrov, G. E. Scuseria, L. A. Constantin, X. Zhou and K. Burke, *Phys. Rev. Lett.*, 2008, **100**, 136406.
37 L. X. Song, J. Xia, Z. Dang, J. Yang, L. B. Wang and J. Chen, *CrystEngComm*, 2012, **14**, 2675
38 Y. P. Chen, C. L. Lu, L. Xu, Y. Ma, W. H. Hou and J. J. Zhu, *CrystEngComm*, 2010, **12**, 3740
39 G. A. Nazri and C. Julien, *Solid State Ionics*, 1992, **53**, 376
40 W. Dong and B. Dunn, *J. Mater. Chem*., 1998, **8**, 665-670.
41 T. Xia, Q. Li, X. Liu, J. Meng and X. Cao, *J. Phys. Chem. B*, 2006, **110**, 2006
42 G. Henkelman, A. Arnaldsson and H. Jónsson, *Comput. Mater. Sci.*, 2006, **36**, 254
43 W. Tang, E. Sanville and G. Henkelman, *J. Phys.: Condens. Mater.*, 2009, **21**, 084204.
44 S. N. Kumar, G. Bouyssoux and F. Gaillard, *Surf. Interface Anal.*, 1990, **15**, 531
45 J. Ma, Q. S. Meng, A. Michelmore, N. Kawashima, Z. Izzuddin, C. Bengtsson and H. C. Kuan, *J. Mater. Chem. A*, 2013, **1**, 4255
46 A. A. Zaman, R. Tsuchiya and B. M. Moudgil, *J. Colloid Interf. Sci.*, 2002, **256**, 73
47 H. Knorke, J. Langer, J. Oomens and O. Dopfer, *Astrophys. J.,* 2009, **706**, 66

